



# Experimental verification of power-law non-Newtonian axisymmetric porous gravity currents

Sandro Longo<sup>1,†</sup>, Vittorio Di Federico<sup>2</sup>, Luca Chiapponi<sup>1</sup>  
and Renata Archetti<sup>2</sup>

<sup>1</sup>Dipartimento di Ingegneria Civile, Ambiente Territorio e Architettura (DICATeA), Università di Parma, Parco Area delle Scienze, 181/A, 43124 Parma, Italy

<sup>2</sup>Dipartimento di Ingegneria Civile, Chimica, Ambientale e dei Materiali (DICAM), Università di Bologna, Viale Risorgimento, 2, 40136 Bologna, Italy

(Received 1 June 2013; revised 18 July 2013; accepted 24 July 2013)

We present a theoretical and experimental analysis of axisymmetric gravity currents of power-law fluids in homogeneous porous media. The non-Newtonian shear-thinning fluid is a mixture of water, glycerol and Xanthan gum ( $n = 0.33\text{--}0.53$ ), and it is injected into a porous layer of glass beads ( $d = 1\text{--}3$  mm). We compare experiments conducted with constant ( $\alpha = 1$ ) and time-increasing ( $\alpha = 1.5$  and  $2.0$ ) influxes to theoretical self-similar solutions obtained by the numerical integration of the nonlinear ordinary differential equation that describes one-dimensional transient motion. The theoretical analysis is confirmed by experimental data. In addition, the selection of the most appropriate expression for the tortuosity factor and the choice of the correct range of shear stress for the determination of the rheological parameters are shown to be crucial to obtaining a good fit between the theory and experiments.

**Key words:** gravity currents, non-Newtonian flows, porous media

## 1. Introduction

Gravity-driven flows in porous media are ubiquitous in environmental and industrial applications, and have been investigated in both the laboratory and in numerous natural contexts. There is a large amount of literature that covers the theoretical analyses and experiments (for a review, see Simpson 1982; Huppert 1986; Ungarish 2010) that pertains to two-dimensional and axisymmetric geometries. In particular, fluid exchanges with geological porous media in a radial geometry have received

<sup>†</sup> Email address for correspondence: [sandro.longo@unipr.it](mailto:sandro.longo@unipr.it)

much attention in connection with groundwater exploitation or remediation, fluid storage in suitable geological units, and reservoir engineering. In several cases, the injected/extracted fluid needs to be treated as non-Newtonian; typical examples include foams and solutions used in enhanced oil recovery, environmental contaminants with nonlinear characteristics, complex substances that are injected into aquifers to act as carriers for remediation agents, and muds that are employed for lubrication in well drilling operations. In a number of instances, the fluid's rheological behaviour is properly described by a Cross or Carreau–Yasuda model (Bird, Stewart & Lightfoot 2002); additionally, this behaviour can be approximated over a limited range of shear rates by the simpler Ostwald–DeWaele model (Bird *et al.* 2002). A study of thin axisymmetric gravity currents of power-law fluids with rheological indices  $n$  in porous media was undertaken by Di Federico, Archetti & Longo (2012), who derived a similarity solution under the assumption of an instantaneous or maintained injection of a fluid volume proportional to  $t^\alpha$ , where the asymptotic rate of spreading was  $\propto t^{(\alpha+n)/(3+n)}$ . This solution generalized the results of Lyle *et al.* (2005). A similar approach was adopted by Pascal & Pascal (1993) and Bataller (2008), who analysed the case of an assigned constant or time-varying level at the origin. In all of these approaches, transient analysis leads to a class of self-similar solutions of a nonlinear advection–diffusion differential equation that has a negative spatial gradient of the free surface in the radial direction. A wider class of self-similar solutions is envisaged for non-Newtonian power-law fluids that spread radially in porous media, and such solutions have already been found for Newtonian fluids (see Chertock 2002).

In this paper, we present an experimental validation of the theoretical predictions for the axisymmetric gravity currents of power-law fluids in porous media. In the next section, the theoretical developments for a current propagating in a homogeneous medium under a shallow water approximation are summarized. Section 3 describes both the experimental setup and the conducted tests and interprets the results. In § 4, the implications of the correct choice of the rheological parameters are discussed.

## 2. Theory

Consider a non-Newtonian fluid with rheological behaviour described by a power-law model for which the shear stress is given by  $\tau = m\dot{\gamma}|\dot{\gamma}|^{n-1}$ , where  $m$  and  $n$  are the consistency and flow behaviour indices, respectively, and  $\dot{\gamma}$  is the shear rate. The fluid has a uniform density  $\rho$  and is released into a homogeneous porous medium that is saturated with a fluid of uniform density  $\rho - \Delta\rho$ . The bottom of the domain is horizontal and impermeable, and the intruding fluid is injected along the vertical axis of the cylindrical coordinate system; this setup is sketched in figure 1, where  $r$  and  $z$  are the radial and vertical coordinates, respectively. Because only axisymmetric flows are considered, the tangential coordinate is not of interest. The interface of the intruding current with the ambient fluid is described by the function  $z = h(r, t)$  and extends from the origin to a radius indicated by  $r_N(t)$ .

For a non-Newtonian power-law fluid, the flow law relating the pressure  $p$  and Darcy velocity  $\mathbf{u}$  can be expressed as:

$$\nabla p - \rho\mathbf{g} = -\frac{\mu_{eff}}{k}|\mathbf{u}|^{n-1}\mathbf{u} \quad (2.1)$$

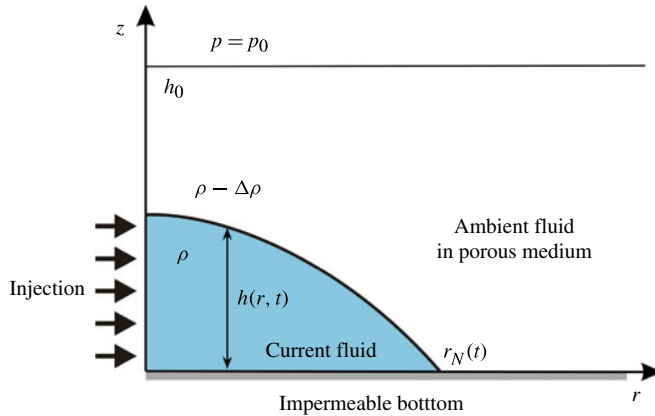


FIGURE 1. A sketch of an axisymmetric gravity current intruding into a saturated porous medium.

where  $\mathbf{g}$  is the gravitational acceleration,  $\mu_{eff}/k$  is the inverse of the mobility,  $\mu_{eff}$  is the effective viscosity and  $k$  is the permeability. The mobility is given by

$$\frac{k}{\mu_{eff}} = \frac{1}{2C_t} \frac{1}{m} \left( \frac{n\phi}{3n+1} \right)^n \left( \frac{50k}{3\phi} \right)^{(n+1)/2} \quad (2.2)$$

where  $\phi$  is the porosity and  $C_t = C_t(n)$  is the tortuosity factor, which can be expressed in several different ways (for a review, see Shenoy 1995). According to Pascal (1983), the tortuosity has the following expression, which was used here to analyse the experimental data:

$$C_t = (25/12)^{(n+1)/2}. \quad (2.3)$$

If we assume that there is a hydrostatic pressure distribution within the intruding fluid and neglect both the dynamics of the ambient fluid and the surface tension effects, the Dupuit approximation (Bear 1972) allows us to express the velocity in (2.1) as

$$u(r, t) = -(\Lambda \Delta \rho g)^{1/n} k^{(1+n)/(2n)} \left| \frac{\partial h}{\partial r} \right|^{1/n-1} \frac{\partial h}{\partial r} \quad (2.4)$$

where

$$\Lambda(\phi, m, n) = \frac{1}{2C_t} \left( \frac{50}{3} \right)^{(n+1)/2} \left( \frac{n}{3n+1} \right)^n \frac{\phi^{(n-1)/2}}{m}. \quad (2.5)$$

The mass balance equation is

$$\frac{1}{r} \frac{\partial}{\partial r} (ruh) + \phi \frac{\partial h}{\partial t} = 0, \quad (2.6)$$

and global continuity requires

$$2\pi\phi \int_0^{r_N(t)} rh(r, t) dr = Qt^\alpha, \quad (2.7)$$

where both  $Q$  and  $\alpha$  are constants. The following boundary condition is imposed at  $r = r_N(t)$ :

$$h(r_N(t), t) = 0. \tag{2.8}$$

By substituting (2.4) into (2.6) and introducing both a velocity scale  $v^* = (\Delta\Delta\rho g)^{1/n} k^{(1+n)/2n} / \phi$  and a time scale  $t^* = (Q/(\phi v^{*3}))^{1/(3-\alpha)}$ , (2.6)–(2.8) can be recast for  $\alpha \neq 3$  as

$$\frac{1}{R} \frac{\partial}{\partial R} \left( RH \frac{\partial H}{\partial R} \left| \frac{\partial H}{\partial R} \right|^{1/n-1} \right) - \frac{\partial H}{\partial T} = 0, \tag{2.9}$$

$$2\pi \int_0^{R_N(T)} RH(R, T) dR = T^\alpha, \tag{2.10}$$

$$H(R_N(T), T) = 0, \tag{2.11}$$

where  $T, R, R_N(T)$  and  $H$  are dimensionless variables. The special case  $\alpha = 3$  requires a different non-dimensionalization and is discussed in Di Federico *et al.* (2012). In the general case, (2.9)–(2.11) admit the following similarity solution:

$$H(R, T) = \eta_N^{n+1} T^{\alpha(n+1)-2n/(3+n)} \psi(\zeta), \quad \zeta = \eta/\eta_N, \tag{2.12}$$

where the new variable is

$$\eta = RT^{-(\alpha+n)/(3+n)}, \tag{2.13}$$

and  $\eta_N$  is its value at  $R_N$ . By substituting (2.12) and (2.13) into (2.9), a nonlinear ordinary differential equation for the function  $\psi(\zeta)$  is obtained:

$$(\zeta \psi \psi' |\psi'|^{1/n-1})' + \frac{n+\alpha}{3+n} \zeta^2 \psi' - \frac{\alpha(n+1)-2n}{3+n} \zeta \psi = 0, \tag{2.14}$$

where the prime indicates  $d/d\zeta$ . Furthermore, the global continuity equation (2.10) transforms into

$$\eta_N = \left( 2\pi \int_0^1 \zeta \psi(\zeta) d\zeta \right)^{-1/(3+n)}, \tag{2.15}$$

and the boundary condition (2.8) becomes

$$\psi(\zeta = 1) = 0. \tag{2.16}$$

For  $\alpha = 0$ , (2.14) and (2.15) have the analytical solutions

$$\psi(\zeta) = \frac{n^n}{(n+1)(n+3)^n} (1 - \zeta^{n+1}), \tag{2.17}$$

$$\eta_N = \left[ \pi \frac{n^n}{(n+3)^{n+1}} \right]^{-1/(3+n)}, \tag{2.18}$$

which, for  $n = 1$ , reduce to the solutions reported in Lyle *et al.* (2005). For a generic value of  $\alpha$ , the solution is obtained by numerical integration, and a necessary second boundary condition can be obtained by developing the asymptotic solution of the Frobenius series near the current tip ( $\zeta = 1$ ):

$$\psi'|_{\zeta \rightarrow 1} = - \left( \frac{\alpha+n}{3+n} \right)^n. \tag{2.19}$$

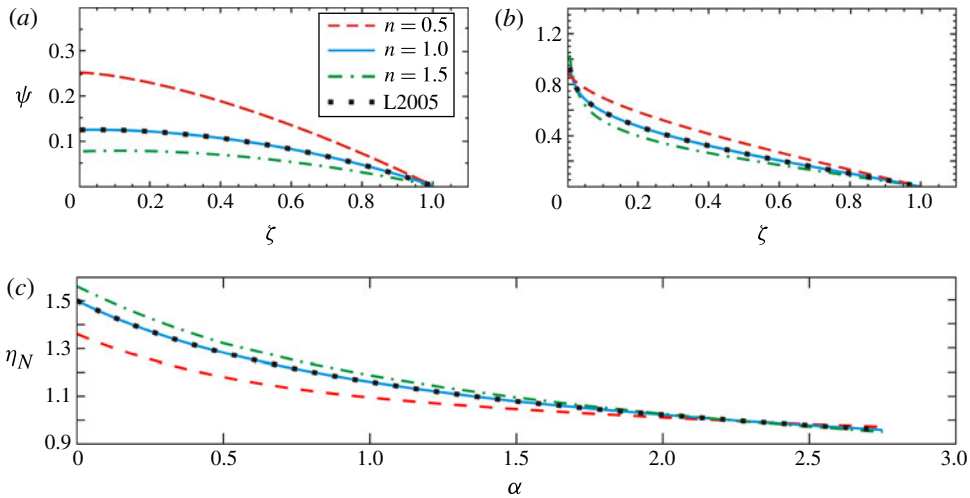


FIGURE 2. Numerical computation of the thickness profile  $\psi$  of the self-similar solutions of an axisymmetric gravity current for shear-thickening (dashed red line), Newtonian (solid blue line), and shear-thinning (dot-dashed line) fluids for (a) a constant volume ( $\alpha = 0$ ) and (b) a constant-flux release ( $\alpha = 1.0$ ). (c) The similarity variable at the current front  $\eta_N$ . The solution for  $n = 1$  reduces to the line that was derived in Lyle *et al.* (2005) (dotted line).

Figure 2 shows the thickness profile  $\psi(\zeta)$  and the dimensionless position  $\eta_N$  of the front end of the current, which is computed numerically for different values of  $n$  and  $\alpha$ . The results indicate that  $\eta_N$  decreases for increasing  $\alpha$  and decreasing  $n$  if  $\alpha \in [0, \approx 2.2]$ . While the origin is an asymptote for the thickness profile if  $\alpha \neq 0$  and  $n \geq 1$ , the function  $\psi(\zeta)$  exhibits a finite slope at the current tip that decreases with increasing  $n$ .

In dimensional variables, the leading edge of the current is given by

$$r_N(t) = \eta_N(\alpha, n) \left( \frac{v^{*n} Q}{\phi} \right)^{1/(3+n)} t^{(\alpha+n)/(3+n)}, \quad (2.20)$$

which is consistent with the correct version of (2.10) in Lyle *et al.* (2005), in which the porosity  $\phi$  is missing. Thus the case  $\alpha = 3$  acts as a discriminant between decelerating and accelerating currents.

### 3. Experiments

To validate the theoretical self-similar solution a series of experiments with constant ( $\alpha = 1$ ) and time-varying influxes ( $\alpha = 1.5$  and  $2.0$ ) were conducted with shear-thinning fluids; the ambient fluid was air for nine tests and water for two tests. Although experiments with Newtonian fluids have already been performed by Lyle *et al.* (2005), three such tests were conducted to check the quality of the experimental protocol and the apparatus.

#### 3.1. The experimental apparatus and protocol

The experiments were performed in a  $90^\circ$  sector glass tank  $25 \text{ cm} \times 25 \text{ cm} \times 25 \text{ cm}$  in size that was filled with transparent glass beads with nominal diameters  $d = 1.0, 2.0$  or  $3.0 \text{ mm}$  and standard deviations of 10% (5% for  $d = 3 \text{ mm}$ ). This setup allowed

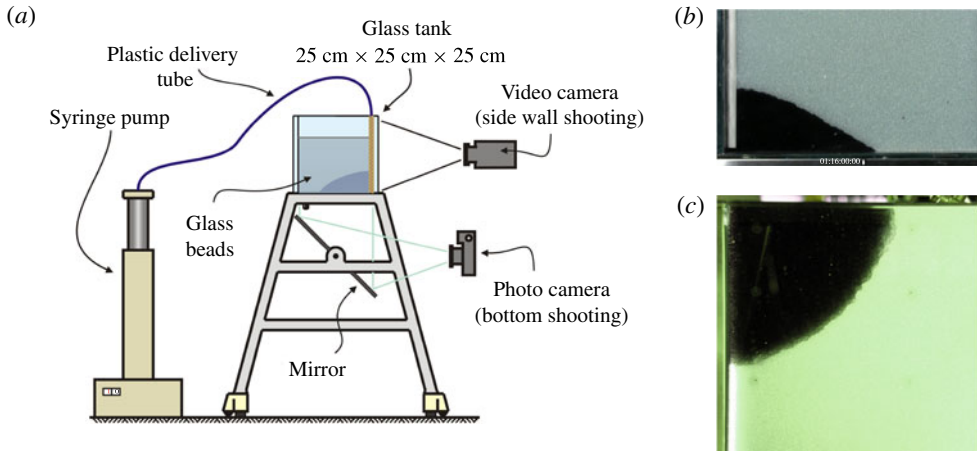


FIGURE 3. (a) The experimental apparatus used for the tests. (b) A snapshot of a constant-flux experiment (side view) and (c) a plane (bottom) view of the same experiment. The results shown are from test 7 for a shear-thinning fluid intruding into a homogeneous porous medium of glass beads with  $d = 1$  mm and air as ambient fluid.

us to observe the time evolution of the intruding current from two lateral sides and through the bottom of the apparatus (figure 3). Two different syringe pumps were used in the experiments. The first pump was self-built in the laboratory and had an estimated accuracy of 1% in the instantaneous discharge. The second was a commercial Teledyne ISCO 260D pump with an accuracy of 0.5%, which could be controlled with an analogue 0–10 V electric signal with 12-bit resolution and was used in all tests with  $\alpha > 1$ . The injection pump was linked to the tank with a rigid tube that had an internal diameter of 6 mm (a tube with a 1 mm internal diameter was used with the second pump) that was positioned vertically at the apex of the tank; the exit section was held 20 mm above the bottom wall. In the second stage of the experiments, a permeable well was constructed along the vertical axis with a brass net to achieve a more realistic reproduction of the theoretical injection mode. The analysis of the experimental results revealed that the different geometries of injection had no significant effect on the thickness profile of the current. For the two tests that used water as the ambient fluid, a weir was inserted into one of the vertical tank walls to discharge the water displaced by the injected volume. The shear-thinning fluids were suspensions of Xanthan gum (0.1% concentration by weight) in water or in a mixture of water and glycerol plus ink to increase the contrast. The rheological properties of the suspensions were preliminarily evaluated to be in the correct range of shear rates (see the discussion in § 4) by two different strain-controlled rheometers: (i) a classical coaxial cylinders shear rheometer (Haake Rotovisco RT10); and (ii) a parallel plate rheometer (Dynamic Shear Rheometer Anton Paar Physica MCR 101). The latter apparatus is more sensitive and accurate at a very low shear rate. The mass density was measured by a hydrometer (STV3500/23 Salmoiraghi) or by weighing a fixed volume of liquid, with an overall accuracy of 1% for both methodologies. In addition, the temperature was systematically measured at the beginning and end of the tests by submerging a mercury-in-glass thermometer with a resolution of 0.02 °C into the current.

Test	$\alpha$	$d$ (mm)	$m$ (Pa s <sup><i>n</i></sup> )	$n$	$\Delta\rho$ (kg m <sup>-3</sup> )	$Q$ (ml s <sup>-1</sup> )
5 <sup><i>a</i></sup>	1.0	3.0	0.68	0.35	1175	0.60
6 <sup><i>a</i></sup>	1.0	2.0	0.68	0.35	1175	0.32
7 <sup><i>a</i></sup>	1.0	1.0	0.80	0.33	1169	0.15
8 <sup><i>a,b</i></sup>	1.0	1.0	0.33	0.48	1000	0.20
9 <sup><i>c</i></sup>	1.0	1.0	0.53	0.53	170	0.04
10 <sup><i>c</i></sup>	1.0	2.0	0.20	0.33	170	0.04
11	1.5	2.0	0.12	0.43	1000	0.06 $t^{1/2}$
12 <sup><i>b</i></sup>	2.0	2.0	0.12	0.43	1000	0.032 $t$
16	1.0	3.0	0.58	1.00	1250	4.00
17	1.0	3.0	0.012	1.00	1145	4.00
18	1.5	3.0	0.26	1.00	1241	0.06 $t^{1/2}$

TABLE 1. The input values for all experiments. The symbol *a* indicates experiments conducted with the pump built in the lab (1% accuracy), the symbol *b* indicates the tests where video is available as supplementary material (see <http://dx.doi.org/10.1017/jfm.2013.389>) and the symbol *c* marks experiments conducted with water as the ambient fluid rather than air.  $Q$  is the full-circle volumetric discharge. The porosity was assumed to be  $\phi = 0.38$ , and the permeability was computed using the Carman–Kozeny relationship. In addition, the values of the rheological parameters were obtained by interpolating the rheometric data at  $\Theta = 25$  °C in the range of 0.1–5 s<sup>-1</sup>.

The instantaneous profile of the current was recorded by a high-resolution video camera (1920 × 1080 pixels) working at 25 frames s<sup>-1</sup> and with a spatial resolution better than 12 pixel mm<sup>-1</sup> under the experimental conditions of the present tests. A photo camera with a resolution of 3456 × 2304 pixels was used to evaluate the radial spreading of the current and to check the overall symmetry by observing the evolution from below. The time step between two consecutive shots of the photo camera varied between 15 and 300 s and depended on the spreading velocity of the current in the different tests. The images were processed with software to obtain a planar restitution and to detect the boundary between the dark intruding current and the light porous medium that had not yet been invaded, with an overall uncertainty of ±1 mm. The images taken from the bottom of the tank were used to evaluate the position of the front end of the current. Table 1 summarizes all the tests that were conducted and the respective input values. Figure 4(*a*) shows the dimensionless radius of propagation as observed from the bottom for all tests as a function of the dimensionless time  $T$  on logarithmic axes. A straight line indicates perfect agreement between the modelled and observed data. Two videos that were taken for tests 8 and 12 are available as supplementary material.

A satisfactory collapse of the data onto the theoretical solution is observed for all tests, which includes those tests with a time-variable influx. Hence the theoretical analysis is confirmed by the experimental data, and the similarity solution and variables are suitable for describing the intrusion process. A more detailed comparison between the theory and our experiments is reported in figure 4(*b*), which depicts the dimensionless thickness profile at different times for a selected test (test 11). A correction was applied to the raw data to take the capillary rise and the meniscus at the glass wall into account. This correction was estimated from specific tests by applying a classical methodology (e.g. Smith, Foote & Busang 1930) for the different diameters of the glass beads and the different liquids used in the experiment.

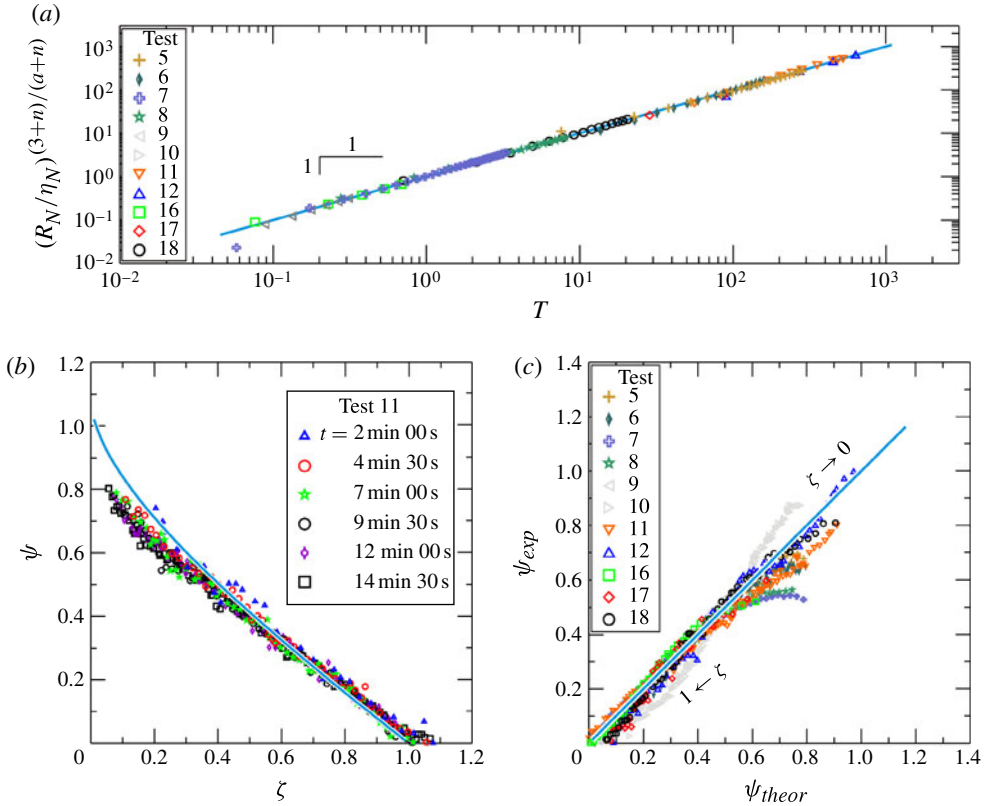


FIGURE 4. A comparison of the theory with our experiments. (a) The dimensionless radius of propagation as a function of the dimensionless time for all tests. The straight lines indicate the perfect agreement with the theory. For clarity, only one point of every two is plotted. (b) The experimental height of the current for a time-increasing influx of a shear-thinning fluid at different times. The thick blue line is the theoretical thickness profile. (c) The experimental thickness profile versus the theoretical thickness profile for all tests, a single profile per test at a time correspondent to the last available shot. The thick blue line indicates perfect agreement with the theory. For clarity, in (b,c) one point of every twenty is plotted.

The correction was equal to  $\approx 1$  or  $\approx 2$  diameters for larger beads and up to 10 diameters for smaller ones with  $d = 1$  mm. However, the time interval necessary to achieve an equilibrium in the capillary rise for the smallest diameter was several tens of minutes, which was often much longer than the duration of the tests. For this reason, the rise of the capillary fringe was monitored over time in separate tests to estimate the appropriate correction to the observed height of the intruding current, which was determined to be proportionate to the time that had elapsed from the start of the injection. Near the origin, the experimental height is systematically below the theoretical one, due to two factors: (i) the disturbances induced by the injection system; and (ii) the intrinsic limitations of the model, which neglects the vertical velocity of the fluid and underestimates the efficiency of the pressure gradient that drives the flow. These model limitations result in an underprediction of the current height near its front end by the continuity equation. In some cases (see figure 4b), this height discrepancy is close to 10 %, whereas the agreement between the theory and our

experiments is nearly perfect in terms of the radius of propagation (figure 4a). This difference is seen because the lateral thickness profiles are the result of a single shot analysis, while the radius of propagation was evaluated as the average distance from the origin over all the points that were detected in the images taken from below. A statistical analysis considering the uncertainties associated with model parameters (see supplementary material) revealed that the experimental data and the theoretical profile are statistically equal with a 95 % level of confidence.

A specific sensitivity analysis was carried out on the tortuosity expression (2.3). Adopting this expression creates an excellent agreement with our experimental results for tests conducted with Newtonian fluids (tests 16, 17, 18), but a systematic reduction of  $\approx 30\%$  is required to reproduce tests with shear-thinning fluids for both constant and time-increasing injections. This result confirms previous findings in the literature on the inherent uncertainty of the tortuosity factor for power-law fluids; the available models and expressions, which are listed in Shenoy (1995), span an interval of variability that is larger than the required correction in the present tests. To apply the tortuosity factor reported by Kemblowski & Michniewicz (1979), a systematic reduction of  $\approx 35\%$  for shear-thinning fluids and of  $\approx 20\%$  for Newtonian fluids is required, whereas the tortuosity factor proposed by Dharmadhikari & Kale (1985) requires a coefficient that ranges from 2.2 to 1.0. Although the tortuosity by Pascal (1983) gives the best fitting with minimum correction, the limited range of the flow behaviour index for the fluids employed in our experiments precluded a more detailed analysis of the correct expression of the tortuosity for power-law fluids. Figure 4(c) shows a comparison between the theoretical and experimental thickness profiles for all tests. Near the front end of the current ( $\zeta \rightarrow 1$ ) the agreement is generally good except for the two tests that employed water as the ambient fluid (i.e. tests 9 and 10); these tests were of long duration, and diffusion mechanisms played a significant role. Therefore detecting the interface between the ambient and intruding fluids was uncertain and difficult, and this issue limited the applicability of the model.

#### 4. Discussion

A relevant issue in our analysis is the selection of appropriate values of the rheological parameters  $m$  and  $n$ , which is also highlighted in Sayag & Worster (2013) for experiments on viscous free-surface gravity currents of power-law fluids. Real non-Newtonian fluids significantly change their rheology at different shear rates, and a power-law expression represents a local approximation of a more complex model. For a suspension of Xanthan gum, a Cross or Carreau–Yasuda model is more appropriate (e.g. Escudier *et al.* 2001). Figure 5(a,b) shows the results of rheometric measurements conducted at three different temperatures on the suspensions of glycerol (60 % vol), water (40 % vol), Xanthan gum (0.1 % weight) and the ink used in tests 5 and 6. Modest shear-thickening behaviour was observed at a very low shear rate for the data measured at  $\Theta = 30^\circ\text{C}$ , which differs from the yield stress or Newtonian behaviour commonly reported in the same range of shear rates for high-concentration Xanthan gum suspensions in water (Whitcomb & Macosko 1978). To the best of our knowledge, such an inversion of the expected rheological behaviour has never been documented and could be relevant as Xanthan gum is largely used in the food industry at concentrations  $>0.5\%$ . As a result most rheometric tests have been conducted on suspensions at this concentration. The few tests on suspensions with a 0.1 % concentration (Helmreich *et al.* 1995) are for shear rates  $>0.5\text{ s}^{-1}$  and with water as a carrier fluid. Because many of the present tests were performed at temperatures less

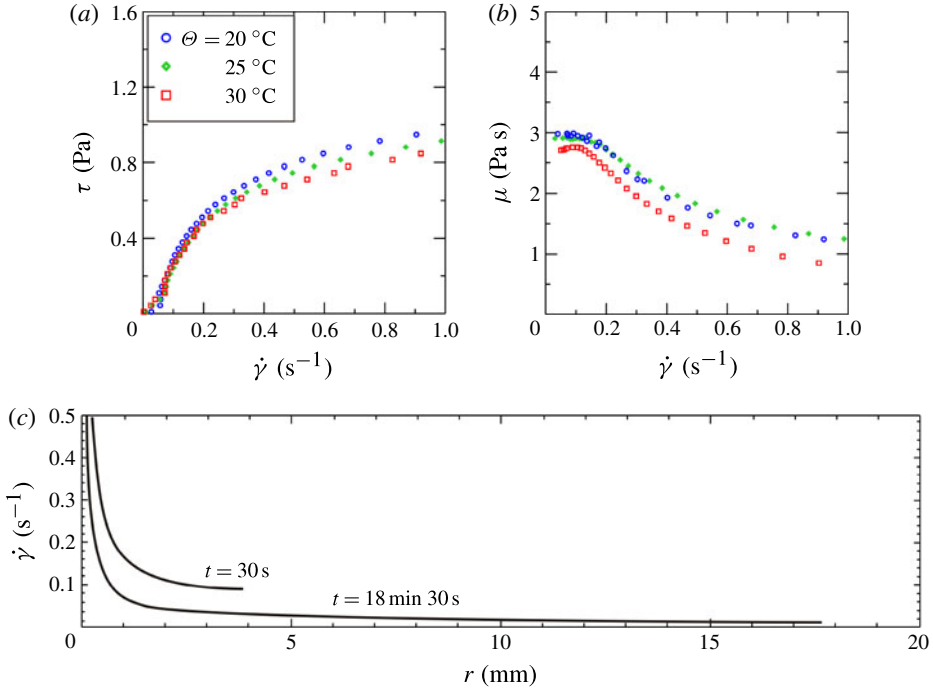


FIGURE 5. (a) Viscometric behaviours of suspensions of glycerol (60% vol), water (40% vol), Xanthan gum (0.1% weight) and ink: the shear stress versus the shear rate. (b) The corresponding apparent viscosities  $\mu = \tau/\dot{\gamma} = m\dot{\gamma}^{n-1}$ . (c) The estimated shear rate at the pore scale for test 5 at times  $t = 30\text{ s}$  and  $t = 18\text{ min } 30\text{ s}$ .

than  $\Theta = 25^\circ\text{C}$ , this apparent anomaly does not affect the present analysis but it is a caveat concerning data interpretation under similar conditions.

To select the correct shear rate range to interpolate the power-law model, it is crucial to evaluate the effective shear rate at the pore scale. An expression to estimate this rate is provided by Savins (1969):

$$\dot{\gamma} = \frac{u\sqrt{2 \times 10^{-4}}}{\sqrt{k\phi c'}}, \quad (4.1)$$

where  $u$  is the Darcian velocity and  $c' = 2.1\text{--}2.4$  is a shift factor related to the tortuosity.

Figure 5(c) shows the estimated shear rate at the pore scale for test 5 both 30 s and 18 min 30 s after the start of the injection. Because the shear rate is very low in most of the flow domain, the power-law parameters should be estimated for  $\dot{\gamma} \rightarrow 0$ . To verify the correctness of this approach, an optimization algorithm was applied to evaluate the two parameters by minimizing the r.m.s. error between the estimates and the experimental data and limiting the computation to portions of the current with  $0.30 < \zeta < 1.0$ . All of the tests systematically yielded values of  $m$  and  $n$  that were larger than the nominal values listed in table 1, and these values were generally in very good agreement with the parameters that were obtained by interpolating the rheometric data in the range of  $0.05\text{--}1\text{ s}^{-1}$ .

## 5. Conclusions

We analysed the axisymmetric gravity currents of Ostwald–DeWaele fluids with a rheological index  $n$  intruding into homogeneous porous media and compared the theoretical results with a set of laboratory experiments. Our self-similar solution extends the analysis performed by Lyle *et al.* (2005) for Newtonian fluids. The experiments for constant ( $\alpha = 1$ ) and variable ( $\alpha = 1.5$  and  $2.0$ ) influxes indicate that the radial spreading of the current is proportional to  $t^{(\alpha+n)/(3+n)}$ , as predicted by the theory. Good agreement between the theory and our experiments is also obtained for the profile and height of the current except near the axis of injection, at which the theoretical vertical asymptote is not present. The choice of the most appropriate expression for the tortuosity factor is essential to obtaining accurate predictions; available formulae for tortuosity seem to overpredict matrix resistance. Because the power-law model is an approximation of the real rheological behaviour, selecting appropriate parameters  $m$  and  $n$  by fitting the rheometric data is crucial. A good agreement between the theory and our experiments is observed by assuming that the relevant shear rate is that measured at the pore scale. The novel results presented in this paper provide a promising basis for the analysis of non-Newtonian gravity currents, which are of practical relevance in environmental and industrial processes.

## Acknowledgement

We thank M. Ungarish for his constructive comments on an earlier version of this paper.

## Supplementary movies/materials

Supplementary movies/materials are available at <http://dx.doi.org/10.1017/jfm.2013.389>.

## References

- BATALLER, R. C. 2008 On unsteady gravity flows of a power-law fluid through a porous medium. *Appl. Maths Comput.* **196**, 356–362.
- BEAR, J. 1972 *Dynamics of Fluids in Porous Media*. Dover.
- BIRD, R. B., STEWART, W. E. & LIGHTFOOT, E. N. 2002 *Transport Phenomena*. John Wiley & Sons.
- CHERTOCK, A. 2002 On the stability of a class of self-similar solutions to the filtration-absorption equation. *Eur. J. Appl. Maths* **13**, 179–194.
- DHRMADHIKARI, R. V. & KALE, D. D. 1985 Flow of non-Newtonian fluids through porous media. *Chem. Engng Sci.* **40**, 527–529.
- DI FEDERICO, V., ARCHETTI, R. & LONGO, S. 2012 Spreading of axisymmetric non-newtonian power-law gravity currents in porous media. *J. Non-Newtonian Fluid Mech.* **189–190**, 31–39.
- ESCUDIER, M. P., GOULDSON, I. W., PEREIRA, A. S., PINHO, F. T. & POOLE, R. J. 2001 On the reproducibility of the rheology of shear-thinning liquids. *J. Non-Newtonian Fluid Mech.* **97**, 99–124.
- HELMREICH, A., VORWERK, J., STEGER, R., MULLER, M. & BRUUN, P. O. 1995 Non-viscous effects in the flow of xanthan gum solutions through a packed bed of spheres. *Chem. Engng J.* **59**, 111–119.
- HUPPERT, H. E. 1986 The intrusion of fluid mechanics into geology. *J. Fluid Mech.* **173**, 557–598.
- KEMBLOWSKI, Z. & MICHNIEWICZ, M. 1979 A new look at the laminar flow of power-law fluids through granular beds. *Rheol. Acta* **18**, 730–739.

- LYLE, S., HUPPERT, H. E., HALLWORTH, M., BICKLE, M. & CHADWICK, A. 2005 Axisymmetric gravity currents in a porous medium. *J. Fluid Mech.* **543**, 293–302.
- PASCAL, H. 1983 Nonsteady flow of non-Newtonian fluids through a porous medium. *Intl J. Engng Sci.* **21**, 199–210.
- PASCAL, J. P. & PASCAL, H. 1993 Similarity solutions to gravity flows of non-Newtonian fluids through porous media. *Intl J. Non-Linear Mech.* **28** (2), 157–167.
- SAVINS, J. G. 1969 Non-Newtonian flow through porous media. *Ind. Engng Chem.* **61**, 18–47.
- SAYAG, R. & WORSTER, M. G. 2013 Axisymmetric gravity currents of power-law fluids over a rigid horizontal surface. *J. Fluid Mech.* **716**, R5–1–11.
- SHENOY, A. V. 1995 Non-Newtonian fluid heat transfer in porous media. *Adv. Heat Transfer* **24**, 102–190.
- SIMPSON, J. E. 1982 Gravity currents in the laboratory, atmosphere, and ocean. *Annu. Rev. Fluid Mech.* **14**, 213–234.
- SMITH, W. O., FOOTE, P. D. & BUSANG, P. F. 1930 Capillary retention of liquid in assemblages of homogeneous spheres. *Phys. Rev.* **36**, 524–530.
- UNGARISH, M. 2010 *An Introduction to Gravity Currents and Intrusions*. CRC.
- WHITCOMB, P. J. & MACOSKO, C. W. 1978 Rheology of xanthan gum. *J. Rheol.* **22**, 493–505.